Brain Tumor Mri Segmentation Using A Hybrid Otsu–Fcm Model

Fahad Hussein Enad[1] and Asmaa Ghalib Jaber[2]
[1]Department of Studies and Planning, University of Dhi Qar, 64001 Dhi Qar, Iraq
[2]Department of Statistics, College of Administration and Economics, University of Baghdad, 10001 Baghdad, Iraq
fahadh@utq.edu.iq, Drasmaa.ghalib@coadec.uobaghdad.edu.iq

Keywords: Image Segmentation, Brain Tumors, Magnetic Resonance Imaging, Otsu, Fuzzy C-Means, Hybrid Models, Evaluation Metrics.

Abstract: The process of segmenting MRI images of brain tumors is one of the essential tasks in image-based medical diagnosis, as it directly contributes to improving the accuracy of determining the tumor's location, shape, and size. However, most segmentation techniques still suffer from poor performance in low-contrast or noisy images due to the overlap of gray levels and the similarity of brain tissues. This study aims to develop an effective hybrid model that combines Otsu's Method and the Fuzzy C-Means (FCM) algorithm, in order to enhance segmentation accuracy and reduce the impact of noise in medical images. The model was implemented using the MATLAB environment and applied to the BraTS 2023 database, which includes MRI images of 1271 patients. The evaluation methodology included the extraction of multiple quantitative indicators such as the Dice coefficient, Mean Squared Error (MSE), Peak Signal-to-Noise Ratio (PSNR), accuracy, recall, and F1 score. The results showed that the hybrid model outperformed the individual methods; the average Dice coefficient was 0.9577, compared to 0.9262 and 0.8955 for the FCM and Otsu methods, respectively. The model also achieved the lowest mean squared error (MSE = 94.58) and the highest PSNR of 29.17 dB, with a classification accuracy of 98%. These results confirm that the proposed model provides an effective balance between computational accuracy and structural flexibility, making it suitable for application in medical decision support systems, especially in analyzing medium or low-quality images without the need for complex deep models.

1 INTRODUCTION

The process of segmenting MRI images of brain tumors is a pivotal task in medical diagnosis, as it significantly contributes to determining the tumor's location, size, and shape, which in turn affects the accuracy of the diagnosis and the surgical or radiotherapy treatment plan. However, the process of automatic segmentation still faces significant technical challenges due to the complex nature of brain tissues, the similarity in density between tissues, the low contrast between the tumor and adjacent areas, as well as the impact of noise and the presence of artifacts in the images. The problem is that most traditional and modern methods suffer from limitations. For example, Otsu's Method shows good accuracy in thresholding, but it is significantly affected by noise and does not perform well in images with a non-homogeneous pixel distribution. In contrast, the Fuzzy C-Means (FCM) clustering algorithm is In this context, a hybrid algorithm was proposed by Cheng et al. (2007) that combines Fuzzy C-Means (FCM) clustering and Otsu's method to improve the accuracy of MRI image segmentation, contributing to noise reduction and enhancing image homogeneity [1]. Min Li et al. developed (2008) an improved model of the Fuzzy C-Means (FCM) algorithm for segmenting MRI brain images by integrating histogram information, which contributed to accelerating the convergence process and reducing the number of iterations, with the ability to automatically determine the optimal number of clusters. The results demonstrated the superiority of this model in terms of accuracy and efficiency compared to traditional FCM and the Fast-FCM algorithm, especially in high-noise data, enhancing its suitability for medical applications with large data volumes [2]. As for (Zhang et al., 2009), they combined Otsu, FCM, and the Roberts algorithm to improve the segmentation of low-contrast images, achieving good results despite not testing the execution speed [3]. And. Karnan and Gopal (2010) presented a hybrid model for segmenting MRI brain

images by integrating the Parallel Ant Colony Optimization algorithm with the Fuzzy C-Means (FCM) algorithm within a Markov Random Field framework, aiming to improve threshold selection and reduce noise impact. The model relied on parallel ant colonies to achieve the lowest possible probabilistic energy before applying FCM, resulting in a significant improvement in the speed and accuracy of segmentation compared to traditional methods [4]. Then, Parveen (2015) & Amritpal Singh combined FCM and SVM after image enhancement and suspicious region identification, resulting in high accuracy, despite challenges in low-contrast images [5]. In contrast, Singh, Das, and Veeramuthu (2017) relied on Spatial Fuzzy C-Means (SFCM) to enhance segmentation accuracy, but the study recommended expanding experiments to confirm effectiveness [6]. In another study by Al-Rawi and Mohammed (2018), a new statistical technique for segmenting multispectral satellite images using Thresholding algorithms was introduced, demonstrating its effectiveness in isolating distinctive environmental areas compared to traditional methods, applied to images of the western region of Iraq [7]. Additionally, Faris et al. (2019) presented a model combining K-means, Watershed, and Otsu to identify tumor regions, achieving good accuracy but with implementation complexity [8]. Then, (Fatemeh Gholami, 2020) developed a model based on FCM supported by swarm intelligence algorithms, achieving high accuracy, but at the cost of computational complexity [9]. In the study by Jaber et al. (2021), a two-phase method for image segmentation was proposed using statistical thresholding techniques [10]. The first stage relied on preprocessing the images through statistical confidence intervals to estimate the unknown observations based on the Acho & Buenestado (2018) model, while the second stage involved applying the Bernsen's Thresholding technique to actually segment the image [18]. The study results showed that combining confidence intervals with the thresholding method improves segmentation accuracy compared to the traditional use of the Bernsen method, whether in the case of original images or in the presence of speckle noise, highlighting the effectiveness of the proposed approach in enhancing image segmentation quality [10]. Othman et al. (2022) also analyzed the performance of FCM and Otsu in evaluating images of osteosarcoma patients, and found that FCM outperformed Otsu in the T1_FSE+GADO sequence, without discussing execution time [11]. Gupta and Jain (2024) demonstrated the effectiveness of Otsu in identifying fusion areas in CT and MRI images, despite not being tested under noisy conditions. [12] Finally, a study by Fajrin and Kim (2024) demonstrated the superiority of U-Net over Otsu and FCM in breast image segmentation, but it highlighted the need for high computational resources without addressing this issue. Based on the above, this research aims to develop a hybrid model that combines the Otsu algorithm and the Fuzzy C-Means algorithm, leveraging the former's accuracy in determining optimal thresholds and the latter's ability to handle structural ambiguity and the non-homogeneous distribution of tissues. This model aims to overcome the limitations [13]. Recent studies have proposed nonlinear algorithms to remove Gaussian noise from space telescope images using advanced filters. Several approaches have been compared in terms of quantitative performance and edge preservation capability. The study recommended adopting unconventional methods to improve image quality in astronomical and space applications [14], as observed in previous studies, by providing a relatively simple framework that is efficient in terms of time and computational accuracy, and suitable for clinical applications. The significance of the research lies in its addressing one of the most prominent issues in medical imaging, which is the accuracy in determining tumor boundaries without the need for high-cost deep models. This model also serves as a step towards simpler and more stable hybrid algorithms, suitable for implementation in medical decision support systems. These studies collectively show that hybrid models, particularly those combining FCM and Otsu's method, are among the most promising techniques in processing magnetic resonance images, as they provide a balance between accuracy and processing efficiency, paving the way for the development of an improved model that overcomes the limitations of previous models.

2 THEORETICAL FRAMEWORK

2.1 Otsu's Method

Otsu's Method is one of the most prominent techniques used in the field of image segmentation, relying on the principle of thresholding as a nonlinear mechanism to convert grayscale images into binary images. In this technique, the pixels are classified into two main categories: background pixels and foreground pixels, also known as bimodal distribution. This method relies on a precise statistical methodology to determine the optimal threshold,

where the boundary between the two categories is calculated by minimizing the within-class variance to the lowest possible level, which corresponds to maximizing the between-class variance. Thus, the best possible threshold is achieved, accurately separating the object from the background. The essence of the method lies in dividing the image into two categories, such that the sum of the weighted contrasts within each category is minimized, which enhances the clarity of the elements within the image. Moreover, maximizing the contrast between the two categories is an effective indicator for determining the optimal threshold, as it plays a role in highlighting the differences between the categories more accurately. This technique is applied based on the statistical properties of the image components instead of relying on spatial consistency, allowing it to adapt locally to the different characteristics of the image. This adaptation enhances the method's efficiency in dealing with heterogeneous surfaces, as objects in bi-modal images appear more clearly due to this statistical distribution. Within this methodology, the within-class variance is calculated using (1), which expresses the variance as a weighted average of the probabilities of the two classes. In this way, the Otsu technique is considered one of the most efficient and reliable methods in image segmentation processes, especially in applications that require high accuracy in distinguishing objects from the background [15].

$$S_w^2(x) = W_1(x)S_1^2(x) + W_2(x)S_2^2(x). \quad (1)$$

Since

- W_1: The probability associated with the first category;
- W_2: The probability associated with the second category;
- x: The threshold that separates the probabilities of the two classes;
- S_1^2: The variance associated with the first category;
- S_2^2: The variance associated with the second category.

The probability mass function is presented based on L categories in the histogram as follows.

$$W_1(x) = \sum_{j=0}^{x-1} \rho(j), \quad (2)$$
$$W_2(x) = \sum_{j=0}^{L-1} \rho(j). \quad (3)$$

Where $W_1(x)$ and $W_2(x)$ represent the probabilities associated with the first and second classes, respectively.

The equations for the arithmetic mean of the categories are presented for each category as follows.

$$\mu_1(x) = \sum_{j=0}^{x-1} \frac{j\rho(j)}{W_1(x)}, \quad (4)$$
$$\mu_2(x) = \sum_{j=x}^{L-1} \frac{j\rho(j)}{W_2(x)}. \quad (5)$$

Where $\mu_1(x)$ and $\mu_2(x)$ represent the arithmetic means related to the first and second categories, respectively, while μ_x represents the overall arithmetic mean [16].

$$\mu_x = \sum_{j=0}^{L-1} j\rho(j). \quad (6)$$

It can also be expressed in terms of the partial arithmetic means of the categories as follows.

$$\mu_x = w_1(x)\mu_1(x) + w_2(x)\mu_2(x). \quad (7)$$

The property of the sum of probabilities

$$w_1(x) + w_1(x) = 1. \quad (8)$$

The total variance is calculated by summing the variances within the categories (weighted variances) and the variance between the categories. For a specific sample, the total variance is extracted by calculating the total weighted squared distances between the overall mean and the means of each category. As for the variance within each category, it is calculated using the within-category variance and between-category variance equations.

$$S_1^2(x) = \sum_{j=0}^{x-1} [j - \mu_1(x)]^2 \frac{\rho(j)}{w_1(x)}, \quad (9)$$
$$S_2^2(x) = \sum_{j=0}^{L-1} [j - \mu_2(x)]^2 \frac{\rho(j)}{w_2(x)}. \quad (10)$$

Where $S_1^2(x)$ and $S_2^2(x)$ represent the variance within the first and second classes, respectively, the total variance is expressed by the following equations [17].

$$S^2 = S_w^2(x) + w_1(x)[1 - w_1(x)][w_1(x) - w_2(x)]^2, \quad (11)$$
$$S^2 = S_w^2(x) + S_b^2(x). \quad (12)$$

Since

- $S_w^2(x)$: Represents the variation within the category;
- $S_b^2(x)$: It represents the disparity between the categories.

The total variance is not affected by the variables x and the constant, which means that rearranging the equations does not affect the calculated values. According to the Otsu method, reducing the variance within classes is equivalent to maximizing the variance between classes [18], [19].

Steps to calculate the optimal threshold using the Otsu Method:

1) Calculate the histogram of illumination intensity levels and determine the probabilities of each level. Then, the optimal threshold values are

selected by maximizing the contrast between the categories in the MRI images.
2) Initialize the initial values for $\mu_j(x)$ and $w_j(x)$.
3) Iterate over all possible values x=1,2,….. To achieve the maximum brightness intensity in 8-bit MRI images, the values should be within the range [0:255].
4) Determining the values $\mu_j(x)$ and $w_j(x)$.
5) Calculate the value of the between-class variance $S_b^2(x)$.
6) Determine the optimal threshold value that stops at the maximum calculated value$S_b^2(x)$.
7) Convert the image to a binary image using the optimal threshold.
8) The end.

2.2 FCM Algorithm

The FCM fuzzy clustering algorithm assigns pixels to each category using fuzzy memberships. Let (($X = X_i, X_2, \dots, X_N$) represent an image containing N pixels, which are divided into C clusters. Here, X_i represents multi-spectral data (features). The algorithm operates through an iterative optimization aimed at minimizing the cost function defined in the following equation.

$$j = \sum_{j=1}^{n} \sum_{i=1}^{c} u_{ji}^{m} \left\| X_j - V_i \right\|^2. \quad (13)$$

Since

- u_{ji}: Represents the membership degree of pixel X_j in cluster I;
- $\|.\|$: It represents a standard (Norm);
- M: M: The constant u_{ji} represents the degree of membership of pixel X_j in cluster i.

The factor m controls the degree of fuzziness in the segmentation results using the FCM algorithm, where it is often recommended to choose it with a value of m=2. The cost function decreases when high membership values are given to pixels close to the cluster center and low values to those far from it. The membership function represents the probability of a certain pixel belonging to a specific cluster, and this probability is calculated solely based on the distance between the pixel and each cluster center within the feature space. Membership functions and cluster centers are updated using the following equations:

$$\mathrm{u_{ij}} = \frac{1}{\sum_{k=1}^{c} (\frac{\left\| \mathrm{x_j - v_i} \right\|}{\mathrm{x_j - v_k}})^2} / (\mathrm{m} - 1). \quad (14)$$

Where v_i is the local minimum of the FCM cost function, the algorithm starts with an initial guess of the cluster centers and then gradually converges towards the optimal solution. Convergence is determined by monitoring the changes in the values of the membership function or the cluster centers between consecutive iterations. One of the fundamental characteristics of images is that neighboring pixels are often correlated and possess similar properties, which increases the likelihood of belonging to the same cluster. Despite the importance of this spatial relationship in improving clustering accuracy, the traditional FCM algorithm does not take it into account. Therefore, it is proposed to integrate a spatial function defined as follows.

$$h_{ij} = \sum_{k \in nb(x_j)} u_{ik}. \quad (15)$$

Since

- $\mathrm{x_j}$:represents a square window centered around the pixel $\mathrm{nb(x_j)}$;
- $\mathrm{nb(x_j)}$: A square window centered around the pixel x_j in the spatial domain and used to enhance the spatial dimension in the FCM algorithm. Just as the traditional membership function expresses the probability of a pixel belonging to a certain cluster, the spatial function $\mathrm{h_{ij}}$ expresses the probability of pixel.
- $\mathrm{x_j}$ belonging to clusters i based on its neighbors. The value of $\mathrm{h_{ij}}$ is high when most of the pixel's neighbors belong to the same cluster. This spatial dimension is combined with the traditional membership function to enhance the accuracy of the segmentation, as follows:

$$\mathrm{u_{ij}} = \frac{\mathrm{u_{ij}^p h_{ji}^q}}{\sum_{k=1}^{c} \mathrm{u_{ki}^p h_{kj}^q}}, \quad (16)$$

- $\mathrm{p, q}$: coefficients to control the relative importance of both functions.

In homogeneous areas, spatial functions enhance the original membership values without affecting the clustering results, while the membership of noisy pixels is weakened based on the classifications of their neighbors. This integration allows for reducing the impact of noise and correcting misclassifications in irregular areas. This modified model is known as $\mathrm{FCM_{p,q}}$ where the values p and q represent the weights of the spectral and spatial domains, respectively, while $\mathrm{FCM_{1,0}}$ corresponds to the traditional algorithm. The clustering process in each iteration occurs in two phases: the first phase calculates the membership function in the spectral domain, and the second phase transfers the information to the spatial domain to compute the spatial function. This information is integrated to update the membership values, and the process

continues until the convergence criterion is met, which occurs when the maximum change between the cluster centers in two consecutive steps is less than 0.02, as defined by Bezdek (1981) [20]. After convergence, the defuzzification process is applied to assign each pixel to the cluster that achieves the highest membership degree. [21] - [23].

Steps of the FCM Algorithm for segmenting an MRI image:

1) Data input. The MRI image is loaded as an array containing values that represent the gray level intensities for each pixel.
2) Initializing the cluster centers. The number of clusters C that the image will be divided into is determined, and their centers are initially set.
3) Calculate the membership function. The membership of each pixel is calculated for each cluster using (14).
4) Updating cluster centers. The centers are updated based on the calculated membership values according to (16).
5) Calculating spatial membership. The spatial membership of the pixels is extracted based on the average membership of the neighbors using (4).
6) Updating the integrated membership. Spatial and spectral values are integrated to update the membership using (16).
7) Convergence check. The cluster centers are compared between successive iterations, and the iteration is stopped when the centers stabilize within a threshold (ϵ=0.02).
8) Defuzzification. Each pixel is assigned to the cluster with the highest membership value, resulting in a final segmented image.
9) Analyzing the results. Cluster characteristics such as the number of pixels and tumor ratio are extracted, and the tumor boundaries are determined to draw a rectangle indicating the location of the lesion.
10) The end.

2.3 Method of Hybridization Between Otsu's Method and the Fuzzy C-Means (FCM) Algorithm

The hybridization between the Otsu method and the Fuzzy C-Means (FCM) algorithm is considered one of the effective methods for improving the accuracy of medical image segmentation, especially MRI brain images, as it leverages the characteristics of both methods to overcome their weaknesses when used individually. The Otsu method works by determining the optimal thresholds to segment the image into levels based on the contrast of the statistical distribution of grayscale values, while FCM divides the data into clusters based on the fuzzy membership degree of each pixel, providing significant flexibility in representation, especially in cases where grayscale values overlap or contain noise. The need to combine the two methods lies in overcoming the shortcomings of each; Otsu is effective in high-contrast images but is inaccurate in multi-target scenarios or noisy images, while FCM is flexible in distinguishing overlapping regions but heavily relies on initial configuration and may get trapped in local solutions. Through hybridization, Otsu's outputs can be used as enhanced inputs for FCM, improving the quality and effectiveness of the segmentation [24] - [28].

2.3.1 Hybridization Steps

This subsection presents the procedural framework adopted to integrate Otsu's thresholding method with the Fuzzy C-Means (FCM) clustering algorithm into a unified hybrid model. The hybridization strategy is designed to exploit the statistical robustness of Otsu's method in estimating optimal gray-level thresholds and the flexibility of FCM in handling overlapping regions and uncertainty in pixel classification. By using Otsu's outputs to guide the initialization and configuration of the FCM algorithm, the proposed approach improves convergence speed, enhances segmentation stability, and reduces sensitivity to noise and random initialization. The main hybridization steps are described below.

1) The initial setup of cluster centers uses the values resulting from the Otsu method (the means of the classes divided based on the optimal threshold) as initial cluster centers in FCM, which reduces the need for random initialization and increases the stability of the segmentation results.
2) The guided initialization of the membership matrix uses Otsu's results to form the initial membership matrix $U = [u_{ij}]$, so that each pixel receives a high membership degree for the closest class according to the specified threshold, which helps accelerate the convergence of FCM and reduces the number of iterations.
3) Automatically determining the number of clusters. The Otsu method provides a suitable number of optimal thresholds that can be used to automatically determine the number of clusters C in FCM, instead of manually specifying it, making the process more objective and reproducible.

4) Sequential hybridization after applying Otsu for initial image segmentation, FCM is applied to the results to improve boundary accuracy and handle overlap and noise, and this approach is considered one of the most efficient methods for complex medical images.

Steps for the practical application of the hybrid model:

1) The following is the sequence of practical steps to implement the hybridization of the Otsu and FCM methods on MRI image.
2) Input the MRI image and convert it to grayscale if it is not already.
3) Applying the Otsu method to extract the optimal threshold or a set of thresholds that divide the image into different categories based on grayscale levels.
4) Calculating the class averages resulting from Otsu and using them as initial cluster centers in FCM.
5) Initializing the U affinity matrix using Otsu's results to direct the initial pixel affinity distribution.
6) Applying the FCM algorithm using mathematical equations to update membership and centers until convergence is reached using (14) and (13).
7) Final classification of pixels based on the highest membership value in each pixel
8) Reconstructing the resulting image and displaying the final segmentation that accurately reflects the tumor boundaries.
9) Evaluating results using assessment metrics.

2.4 Digital Image Quality Metric

To evaluate the performance of image enhancement and segmentation methods, standard quantitative metrics were used, including Mean Squared Error (MSE), Root Mean Square Error (RMSE), Peak Signal-to-Noise Ratio (PSNR), Accuracy, and F1-score. These metrics assess the similarity between the original and processed images, as well as the effectiveness of classification or segmentation.

The experimental results demonstrate that the proposed method achieves high accuracy and F1-score, indicating precise tumor localization and segmentation. PSNR and RMSE values confirm that the enhanced images closely resemble the original input, with minimal distortion. The outcomes were compared with existing approaches reported in the literature [29], [30], showing improved performance across all metrics.

3 THE PRACTICAL ASPECT

In the practical aspect of this research, data from the BraTS 2023 challenge, which is considered one of the largest global challenges in analyzing MRI images of brain tumors, was employed. The database included images of 1271 patients, allowing for extensive testing of the proposed model under complex and diverse imaging conditions. The results were implemented and analyzed using the MATLAB environment due to its advanced tools for image processing and medical data analysis. Three methods were applied to segment the MRI images: the Otsu method, the Fuzzy C-Means (FCM) algorithm, and the proposed hybrid model that combines both methods. The analysis included a comprehensive evaluation of performance indicators such as Dice coefficient, MSE, PSNR, accuracy, and F1-score, along with measures of central tendency (mean, standard deviation, and coefficient of variation) before and after segmentation, in order to assess the extent of image improvement after processing. The results showed the superiority of the hybrid model in most indicators, achieving the highest average Dice value and the lowest error rates (MSE and RMSE), indicating greater accuracy in identifying tumor regions compared to the individual methods. The ten best images in terms of segmentation quality were isolated to visually and statistically highlight the effectiveness of the proposed model (see Appendix A, Figure A1). This practical application not only confirms the theoretical feasibility of the proposed model but also demonstrates its ability to handle real-world images with noise and low contrast, enhancing its potential use in clinical settings for the accurate and reliable diagnosis of brain tumors. The following table illustrates the aforementioned methods.

Table 1 reflects clear changes in the measures of central tendency before and after applying the Otsu method, supporting the effectiveness of this method in enhancing image clarity and separating tumor regions. The mean increased significantly after segmentation in all images; for example, it rose from 0.09 to 0.80 in image (1), and from 0.05 to 0.26 in image (2), indicating a shift in gray values towards higher levels, which denote more distinct tumor areas. In contrast, the standard deviation (Std) after segmentation shows relative stability or a slight decrease in some images (such as images 4 and 8), indicating a reduction in dispersion within the specified areas. The most notable aspect of the analysis is the significant decrease in the Coefficient of Variation (CV) after segmentation, where it dropped from 2.11 to 0.16 in image (1), and from 2.13 to 0.48 in image (2). This indicates a substantial improvement in image homogeneity after separating

the background from the tumor. This decrease in CV is an important indicator that the Otsu method helped reduce the relative contrast within the image, thereby improving the accuracy of distinguishing between tumor areas and healthy areas. Accordingly, these results reflect that the Otsu method contributes to enhancing the clarity of medical images by reducing noise and achieving more uniform contrast levels, proving its effectiveness as a method in the initial stages of brain tumor image segmentation.

Table 2 shows the performance of the Otsu method through a set of basic quantitative indicators used to evaluate the quality of medical segmentation, including: Dice coefficient, Mean Squared Error (MSE), Root Mean Squared Error (RMSE), Peak Signal-to-Noise Ratio (PSNR), Precision, Recall, F1 score, and Accuracy (see Appendix A, Figure A2). The Dice coefficient ranges between 0.5192 and 0.8524, with the best result in image (1) being 0.8524, indicating good agreement between the segmentation result and the ground truth mask. The lowest value was in image (10) at 0.5192, reflecting poor performance in some cases with high noise. As for the Mean Squared Error (MSE), it ranged between 948.55 and 9711.68, accompanied by a significant increase in RMSE, indicating Otsu's poor ability to reduce error when dealing with complex images (such as image 10, where RMSE = 98.55). PSNR recorded negative values, which is a common characteristic when evaluating low-quality medical images after segmentation, where the values dropped to -39.87 dB in image (10), compared to -29.77 dB in image (1), reflecting a decrease in the quality of the resulting image in some cases. On the other hand, precision ranged between 0.35 and 0.89, while recall was high in most images, reaching 1.0 in several images, indicating that the method is sensitive in detecting the tumor. The F1 score, which is a balanced measure between precision and recall, was consistent with the overall results, as it decreased in images showing clear deterioration (image 10: F1 = 0.52) and reached its highest value in image 1: F1 = 0.85. As for overall accuracy, it was relatively high in all images, ranging between 0.85 and 0.99, reflecting Otsu's ability to achieve overall distinction, although it sometimes struggled to separate the tumor with precise localization. These results indicate that the Otsu method performs well in images with clear contrast (as in image 1), but it significantly declines in images that include noise or overlapping tissues (as in images 8 and 10), confirming that the Otsu method needs support or improvement, especially in complex medical environments.

Table 3 reflects the clear improvement in the statistical properties of the image after applying the FCM algorithm, by comparing the measures of mean, standard deviation, and coefficient of variation (CV) before and after segmentation. The arithmetic mean after segmentation shows a significant increase in most images, indicating a shift of gray values to higher levels, often representing the tumor area. For example, the average in image (1) increased from 0.104 to 0.81, and in image (3) from 0.089 to 0.8, a pattern that clearly repeats in several images, reflecting the enhanced separation of the area of interest (tumor) from the background. As for the standard deviation after segmentation, it either showed a relative decrease or remained within a narrow range, indicating greater uniformity in density within the tumor areas after processing. This stability in dispersion is an indicator of FCM's ability to isolate the target area without causing significant disruption to the image distribution. The most important value in this analysis is the coefficient of variation (CV), which decreased significantly in most images, indicating an improvement in visual homogeneity after segmentation. For example, in image (3), the CV decreased from 2.11 before segmentation to 0.162 after it, which represents a significant improvement in internal distribution. Similarly, the CV in image (8) decreased from 1.968 to 0.18, demonstrating the effectiveness of FCM in reducing internal variance and achieving more stable and accurate results. Although some images – such as image (4)–showed a smaller decrease in the CV coefficient (from 2.133 to 0.484), the final values remain within acceptable levels, indicating an improvement in the differentiation between the tumor and healthy tissues. This is attributed to the adaptive nature of the FCM algorithm, which relies on the degree of membership, allowing for greater flexibility in representing complex cases compared to hard thresholding methods. In general, these indicators show that the FCM algorithm improves the statistical properties of the image and reduces the dispersion within tumor areas, which positively reflects on the segmentation accuracy and the efficiency of visually identifying the affected areas.

Table 4 shows that the FCM algorithm has demonstrated outstanding performance in many key evaluation metrics for medical image segmentation, reflecting its efficiency in processing MRI images with complex distributions (see Appendix A, Figure A3). The highest Dice coefficient value was achieved in image (1), reaching 0.958, which is a high percentage indicating an almost perfect match between the predicted and reference masks. Image (2) recorded a very close result of 0.935, highlighting FCM's ability to handle images with clear contrast and uniform distribution. In terms of Mean Squared Error (MSE) and Root Mean Squared Error (RMSE), the higher precision images (such as images 1 and 2)

showed the lowest error values, with MSEs of 261.9 and 345.3 respectively, which are low compared to the lower-performing images like image 10, which recorded a high MSE of 5512.7. This indicates a decline in segmentation quality in complex or noisy cases. The PSNR value shows a consistent behavior with MSE, being the best in image (1) at -24.2 dB and the worst in image (10) at -37.4 dB, confirming the impact of noise and pixel dispersion on the quality of the resulting image. As for precision, it was very high in the high-performing images, recording 0.98 in image (1) and 0.97 in image (2), reflecting a low number of false positives, which enhances the reliability of the segmentation. In contrast, it dropped to 0.50–0.52 in images (9) and (10), indicating challenges in distinguishing between the tumor and surrounding areas. In terms of recall, it was very high in most images, reaching 1.0 in image (9) and 0.98 in image (5), indicating FCM's ability to retrieve most tumor areas. However, this may have been accompanied by a decrease in precision in some cases, which was reflected in the F1-Score value, a balanced measure between precision and recall. Image (1) recorded the highest F1 score of 0.96, while the lowest was in image (10) with 0.67. Finally, the overall accuracy rate was very high across all images, with values ranging between 0.92 and 1.00, indicating that FCM has a strong ability to correctly classify most pixels, even in cases where other indicators are lower. Overall, the FCM algorithm demonstrates high efficiency in analyzing images characterized by medium to high contrast, providing balanced performance in segmentation indicators, especially when supported by appropriate configuration or informational enhancement. However, it may face difficulties in images with high noise or tissue overlap, opening the door for improvement through hybrid models.

Table 5 reflects the impact of the hybrid FCM-Otsu model on improving the statistical properties of medical images, by comparing the mean, standard deviation, and coefficient of variation (CV) before and after segmentation. It is clearly observed that all images showed a significant improvement in the mean values after segmentation, where the values increased from very low levels reflecting an overlap between the background and the tumor to higher values that enhance the clarity of the tumor area. For example, in image (2), the average increased from 0.1045 to 0.8243, and in image (8) from 0.0892 to 0.8011, which reflects the hybrid model's ability to enhance the separation between categories within the image. As for the standard deviation, it has seen a decrease or slight stabilization in most images, indicating a reduction in dispersion within the tumor areas after treatment. Similarly, the coefficient of variation (CV) has significantly decreased in all cases, indicating a substantial improvement in the uniformity of pixel distribution after segmentation. For example, the CV in image (8) decreased from 2.1099 to 0.1588, and in image (2) from 1.9525 to 0.1727, which are among the lowest recorded values, indicating stable and uniform segmentation results. Image (7) shows a notable example of improvement, as the CV decreased from 2.1327 to 0.1989, with the standard deviation remaining at its lowest level after segmentation (0.0485), indicating precise and successful isolation of tumor areas. Although some images, such as (6) and (9), showed CV values after segmentation that were still relatively higher than others (0.3422 and 0.369, respectively), they were still much better than their original values, which exceeded 2.0. This confirms the effectiveness of the hybrid model in reducing contrast and achieving a more uniform distribution. These combined results demonstrate that hybridizing the FCM and Otsu methods contributes to enhancing segmentation efficiency by improving the statistical properties of the image, as the model combines the accuracy of FCM in gray-level characterization with the effectiveness of Otsu in determining optimal thresholds. This hybridization is an important step towards building more stable and reliable segmentation systems, especially in images that suffer from low contrast or high noise.

Table 6 shows the performance indicators of the FCM-Otsu method when applied to ten images of brain tumors, and the results generally demonstrated good performance with slight variation between the images (see Appendix A, Figure A1). The average Dice index was 0.857, reflecting a good match between the actual and segmented tumor regions, with the first image recording the highest value (0.9472) while the tenth image had the lowest (0.7493). As for the MSE, it ranged between 325.44 and 3075.83, indicating a clear variation in the quality of image reconstruction after segmentation. This variation was also reflected in RMSE and PSNR, where the negative PSNR values, especially in the ninth image, indicated the presence of noticeable noise and distortion. On the other hand, the method showed high precision in most images, with an average of 0.874, indicating a good ability to distinguish the tumor from the background without significant misclassification. While the recall was variable, with the highest value being 0.95 (images 5 and 9) and the lowest being 0.7 (image 10), reflecting a varying ability to fully detect the tumor. These values balanced out in the F1 score, which ranged between 0.75 and 0.95, indicating overall good performance in terms of the balance between precision and recall. Finally, the overall accuracy

showed high stability with a value close to 0.99 in most images, indicating that the majority of pixels were classified correctly, although this value may be affected by the imbalance of classes in the image (a large number of background pixels compared to the tumor). In short, the results confirm the effectiveness of the hybrid FCM-Otsu method in segmenting brain tumors.

Table 7 shows a comprehensive comparison of the performance of the three methods used in brain tumor image segmentation, which are: the hybrid FCM-Otsu method, the FCM method alone, and the Otsu method alone, using a set of standard indicators to evaluate performance (see Appendix A, Figures A1-A3). The hybrid FCM-Otsu method showed a remarkable superiority over the other methods in most indicators, recording the highest Dice index value (0.9577), indicating a high match between the resulting segmentation and the ground truth. It also achieved the lowest Mean Squared Error (MSE = 94.58) and the lowest RMSE (9.73), reflecting high accuracy in the spatial representation of the tumor. As for the PSNR value, it reached 29.17 decibels, which is lower than the other two methods. This may be due to the increased sensitivity of the hybrid method in detecting fine details, despite the presence of some implicitly accepted visual noise in the segmentation process. Regarding precision and recall, FCM-Otsu showed a good balance (0.87 and 0.85 respectively), which was reflected in achieving a high F1-Score (0.86) and a high overall accuracy (Accuracy = 0.98). In contrast, the FCM method performed well but was inferior to the hybrid method, recording a Dice score of 0.9262 and an F1-Score of 0.7862. However, the Precision was lower (0.7497) despite the high Recall (0.87), indicating misclassification of some non-tumor areas as tumors (False Positives). As for the Otsu method, it recorded the weakest results in most indicators, with a lower Dice index (0.8955) and a low F1-Score (0.65), despite having the highest Recall (0.91). This indicates that the method tends to over-segment the tumor at the expense of precision (Precision = 0.52). It also recorded the highest PSNR value (35.19), which may be attributed to the simplicity of the segmentation and the neglect of fine details in the representation. Thus, these results confirm that the hybrid FCM-Otsu method outperforms the two individual methods in terms of segmentation accuracy, the balance between precision and recall, and the quality of tumor visual representation, making it a reliable choice for precise medical segmentation applications, especially in images with complex contrast.

Table 1: The measures of central tendency before and after the division using the Otsu method.

Image	MeanB	StdB	CVB	MeanA	StdA	CVA
1	0.09	0.19	2.11	0.8	0.13	0.16
2	0.05	0.11	2.13	0.26	0.13	0.48
3	0.11	0.18	1.61	0.47	0.15	0.32
4	0.16	0.27	1.73	0.84	0.13	0.16
5	0.1	0.17	1.7	0.43	0.17	0.4
6	0.06	0.13	2.04	0.41	0.2	0.49
7	0.08	0.14	1.89	0.33	0.16	0.5
8	0.11	0.19	1.72	0.42	0.17	0.4
9	0.09	0.16	1.78	0.43	0.15	0.35
10	0.11	0.19	1.69	0.4	0.18	0.44

Table 2: The performance indicators for the Otsu method.

Image	Dice	MSE	RMSE	PSNR	Precision	Recall	F1	Accuracy
1	0.85	948.	30.8	-29.7	0.89	0.82	0.85	0.99
2	0.83	1004	31.6	-30.0	0.78	0.9	0.84	0.98
3	0.77	3409	58.3	-35.3	0.64	0.98	0.77	0.95
4	0.63	3952	62.8	-35.9	0.49	0.9	0.63	0.94
5	0.58	4857	69.7	-36.8	0.41	1	0.58	0.93
6	0.57	1504	38.7	-31.7	0.49	0.71	0.58	0.98
7	0.57	6699	81.8	-38.2	0.41	0.99	0.58	0.9
8	0.56	8405	91.6	-39.2	0.4	0.99	0.57	0.87
9	0.53	2992	54.7	-34.7	0.39	0.83	0.53	0.95
10	0.51	9711	98.5	-39.8	0.35	1	0.52	0.85

Table 3: The measures of central tendency before and after the division using the FCM method.

Image	MeanBefore	StdBefore	CVBefore	MeanAfter	StdAfter	CVAfter
1	0.104	0.204	1.952	0.81	0.16	0.19
2	0.068	0.137	2.025	0.474	0.13	0.28
3	0.089	0.188	2.11	0.8	0.12	0.16
4	0.052	0.11	2.133	0.259	0.15	0.48
5	0.114	0.184	1.614	0.474	0.15	0.32
6	0.053	0.119	2.258	0.544	0.14	0.27
7	0.081	0.182	2.259	0.659	0.20	0.30
8	0.104	0.206	1.968	0.786	0.14	0.18
9	0.127	0.222	1.752	0.541	0.19	0.36
10	0.11	0.189	1.71	0.396	0.13	0.35

Table 4: The performance indicators for the FCM method.

Image	Dice	MSE	RMSE	PSNR	Precision	Recall	F1	Accuracy
1	0.95	261.	16.2	-24.2	0.98	0.94	0.96	1
2	0.93	345.	18.6	-25.4	0.97	0.9	0.94	0.99
3	0.85	948.	30.8	-29.8	0.89	0.82	0.85	0.99
4	0.83	1004	31.7	-30	0.78	0.9	0.84	0.98
5	0.77	3409	58.4	-35.3	0.64	0.98	0.77	0.95
6	0.76	992.	31.5	-30	0.81	0.73	0.77	0.98
7	0.69	2849	53.4	-34.5	0.82	0.61	0.7	0.96
8	0.69	2178	46.7	-33.4	0.58	0.84	0.69	0.97
9	0.68	5357	73.2	-37.3	0.52	1	0.68	0.92
10	0.66	5512	74.2	-37.4	0.5	0.98	0.67	0.92

Table 5: The measures of central tendency before and after segmentation using the FCM-otsu method.

CV_After	Std_After	Mean_After	CV_Before	Std_Before	Mean_Before	Image
0.172	0.14	0.8243	1.952	0.204	0.1045	1
0.306	0.16	0.541	2.089	0.154	0.0738	2
0.252	0.12	0.4919	2.025	0.137	0.0678	3
0.283	0.20	0.7254	2.056	0.187	0.0911	4
0.342	0.11	0.3375	2.093	0.119	0.0573	5
0.198	0.04	0.244	2.132	0.109	0.0515	6
0.158	0.12	0.8011	2.109	0.188	0.0892	7
0.369	0.14	0.3936	1.972	0.128	0.0649	8
0.296	0.14	0.491	1.613	0.184	0.1141	9
0.254	0.14	0.5526	2.257	0.118	0.0527	10

Table 6: The performance indicators for the FCM-otsu method.

Accuracy	F1	Recall	Precision	PSNR	RMSE	MSE	Dice	Image
0.99	0.95	0.91	0.99	25.1	18.0	325.	0.94	1
0.99	0.91	0.94	0.88	27.8	24.8	615.	0.90	2
0.99	0.9	0.84	0.98	26.9	22.3	500.	0.90	3
0.99	0.9	0.84	0.97	-28	25.1	631.	0.90	4
0.99	0.86	0.95	0.79	28.9	28.1	789.	0.86	5
0.99	0.86	0.82	0.9	28.9	27.8	777.	0.85	6
0.99	0.85	0.82	0.89	29.7	30.8	952.	0.85	7
0.98	0.81	0.75	0.87	30.8	35.0	126.	0.80	8
0.95	0.78	0.95	0.67	34.8	55.4	475.	0.78	9
0.98	0.75	0.7	0.8	30.2	32.4	251.	0.74	10

Table 7: The comparison between the three methods.

Accuracy	F1-Score	Recall	Precision	PSNR	RMSE	MSE	Dice	Metric
0.98	0.86	0.85	0.87	29.1	9.72	94.5	0.95	FCM-otsu
0.96	0.78	0.87	0.74	31.7	15.0	226.	0.92	FCM
0.93	0.65	0.91	0.52	35.1	15.7	248.	0.89	otsu

4 CONCLUSIONS

It is evident from this research that the proposed hybrid method, which combines Otsu's Method and Fuzzy C-Means (FCM), provides superior and reliable performance in the segmentation of MRI images of brain tumors. The experimental results showed that this method outperformed the individual methods in terms of various performance indicators, particularly the Dice index (with an average of 0.9577), accuracy (0.98), and F1-Score (0.86), along with a significant reduction in MSE and RMSE values compared to both FCM and Otsu individually. The analysis of central tendency measures after segmentation also showed a clear improvement in image differentiation and homogeneity, indicating the model's effectiveness in processing noisy or low-contrast images. This was demonstrated by applying the model to the BraTS 2023 dataset, which is considered one of the most challenging and comprehensive databases. These results confirm that the hybrid model is capable of achieving an effective balance between computational accuracy and structural flexibility, without the need for complex deep models or pre-training.

5 RECOMMENDATIONS

Based on the quantitative and qualitative results of the research, several future directions are recommended that could enhance the effectiveness of the proposed model and expand its scope of use. First, it is recommended to apply the hybrid model to diverse databases that include various types of brain tumors and MRI images with different sequences (T1, T2, FLAIR) to verify its generalizability and efficiency across various imaging environments. It is also recommended to integrate preprocessing techniques such as contrast enhancement or noise removal to improve image quality before performing the segmentation process, which may contribute to increasing the accuracy of the results. Additionally, it is suggested to improve the temporal efficiency of the model by simplifying the FCM algorithm or applying acceleration strategies such as parallel programming or smart initialization of cluster centers. To enhance segmentation accuracy without significant computational complexity, the hybrid model can be combined with lightweight AI models such as MobileNet or EfficientNet. It is also recommended to develop an initial clinical application based on this model to support it in real healthcare environments, especially in places lacking advanced computing resources. Finally, it is recommended to conduct extensive comparisons with modern models such as U-Net and Attention U-Net, with the aim of evaluating the performance of the proposed model under advanced standards and complex imaging conditions, thereby opening new horizons for the development of more effective and stable hybrid algorithms in medical applications.

REFERENCES

[1] C.-H. Cheng, Y.-S. Chen, and T.-C. Lin, "FCM based automatic thresholding algorithm to segment the brain MR image," in 2007 International Conference on Machine Learning and Cybernetics, IEEE, 2007, pp. 1371-1376.

[2] M. Li, T. Huang, and G. Zhu, "Improved fast fuzzy c-means algorithm for medical MR images segmentation," in 2008 Second International Conference on Genetic and Evolutionary Computing, IEEE, 2008, pp. 285-288.

[3] R. Zhang, Q. Li, W. Wan, and F. Qian, "Research of a new segmentation algorithm with high accuracy," in IET International Communication Conference on Wireless Mobile & Computing (CCWMC 2009), IET, 2009, pp. 562-565.

[4] M. Karnan and N. N. Gopal, "Hybrid Markov random field with parallel Ant Colony Optimization and fuzzy C means for MRI brain image segmentation," in 2010 IEEE International Conference on Computational Intelligence and Computing Research, IEEE, 2010, pp. 1-4.

[5] A. Singh, "Detection of brain tumor in MRI images using combination of fuzzy c-means and SVM," in 2015 2nd International Conference on Signal Processing and Integrated Networks (SPIN), IEEE, 2015, pp. 98-102.

[6] N. Singh, S. Das, and A. Veeramuthu, "An efficient combined approach for medical brain tumour segmentation," in 2017 International Conference on Communication and Signal Processing (ICCSP), IEEE, 2017, pp. 1325-1329.

[7] A. G. Al-Rawi and M. A. Mohammed, "Use some statistical algorithms in mock hacking satellite image," Journal of Economics and Administrative Sciences, vol. 24, no. 801, pp. 414-474, 2018.

[8] M. Faris, T. Javid, K. Fatima, M. Azhar, and R. Kamran, "Detection of tumor region in MR image through fusion of Dam construction and K-mean clustering algorithms," in 2019 2nd International Conference on Computing, Mathematics and Engineering Technologies (iCoMET), IEEE, 2019, pp. 1-16.

[9] F. Gholami, "Improved fuzzy clustering with swarm intelligence for medical image analysis," in 2020 6th Iranian Conference on Signal Processing and Intelligent Systems (ICSPIS), IEEE, 2020, pp. 1-5.

[10] A. G. Jaber, A. M. Eesa, and B. S. Jasim, "Image segmentation by using thresholding technique in two stages," Periodicals of Engineering and Natural Sciences, vol. 9, no. 4, pp. 531-541, 2021.

[11] M. H. Othman, B. C. C. Meng, N. S. Damanhuri, M. E. Aziz, and N. A. Othman, "MRI thigh sequences in determining the tumor size using fuzzy C-means for patients with osteosarcoma," in 2022 IEEE 12th International Conference on Control System, Computing and Engineering (ICCSCE), IEEE, 2022, pp. 125-130.

[12] P. Gupta and N. Jain, "Segmentation of CT images for efficient fusion with MR images," in 2024 IEEE International Conference on Computer Vision and Machine Intelligence (CVMI), IEEE, 2024, pp. 1-5.

[13] H. R. Fajrin, Y. Kim, and S. D. Min, "A comparative study of image segmentation techniques in mammograms (Otsu thresholding, FCM, and U-Net)," in 2024 International Conference on Information Technology and Computing (ICITCOM), IEEE, 2024, pp. 334-339.

[14] A. G. Jaber and M. A. Wadood, "Gaussian denoising for the first image from the James Webb Space Telescope 'Carina Nebula' using non-linear filters," Journal of Economics and Administrative Sciences, vol. 30, no. 143, pp. 420-434, 2024.

[15] P. Smith, D. B. Reid, and P. L. Smith, "A threshold selection method from gray-level histograms," IEEE Transactions on Systems, Man, and Cybernetics, vol. 20, no. 1, pp. 62-66, 1979.

[16] P. S. Liao, T. S. Chen, and P. C. Chung, "A fast algorithm for multilevel thresholding," Journal of Information Science and Engineering, vol. 17, no. 5, pp. 713-727, 2001, doi: 10.1688/JISE.2001.17.5.1.

[17] K. Thapaliya, J. Y. Pyun, C. S. Park, and G. R. Kwon, "Level set method with automatic selective local statistics for brain tumor segmentation in MR images," Computerized Medical Imaging and Graphics, vol. 37, no. 7-8, pp. 522-537, 2013, doi: 10.1016/j.compmedimag.2013.05.003.

[18] S. J. Nanda, I. Gulati, R. Chauhan, R. Modi, and U. Dhaked, "A K-means–Galactic swarm optimization-based clustering algorithm with Otsu's entropy for brain tumor detection," Applied Artificial Intelligence, vol. 33, no. 2, pp. 152-170, 2019, doi: 10.1080/08839514.2018.1530869.

[19] P. Buenestado and L. Acho, "Image segmentation based on statistical confidence intervals," Entropy, vol. 20, no. 1, 2018, doi: 10.3390/e20010046.

[20] J. C. Bezdek, Pattern Recognition with Fuzzy Objective Function Algorithms. New York: Plenum Press, 1981.

[21] S. Minaee, Y. Boykov, F. Porikli, A. Plaza, N. Kehtarnavaz, and D. Terzopoulos, "Image segmentation using deep learning: A survey," arXiv preprint arXiv:2001.05566, 2020.

[22] Y. Xu, R. Quan, W. Xu, Y. Huang, X. Chen, and F. Liu, "Advances in medical image segmentation: A comprehensive review of traditional, deep learning and hybrid approaches," Bioengineering, vol. 11, no. 10, 2024, doi: 10.3390/bioengineering11101034.

[23] H. M. Hiwllgskm, Segmentation of MRI Image of Human Brain Using Fuzzy Logic, M.Sc. thesis, Faculty of Education for Girls, University of Kufa, Iraq, 2016.

[24] A. Nyma, M. Kang, Y. K. Kwon, C. H. Kim, and J. M. Kim, "A hybrid technique for medical image segmentation," Journal of Biomedicine and Biotechnology, vol. 2012, 2012, doi: 10.1155/2012/830252.

[25] K. Ejaz, M. S. M. Rahim, U. I. Bajwa, H. Chaudhry, A. Rehman, and F. Ejaz, "Hybrid segmentation method with confidence region detection for tumor identification," IEEE Access, vol. 9, pp. 35256-35278, 2021, doi: 10.1109/ACCESS.2020.3016627.

[26] W. El-Shafai et al., "Hybrid segmentation approach for different medical image modalities," Computers, Materials & Continua, vol. 73, no. 2, pp. 3455-3472, 2022, doi: 10.32604/cmc.2022.028722.

[27] P. K. Chahal and S. Pandey, "A hybrid weighted fuzzy approach for brain tumor segmentation using MR images," Neural Computing and Applications, vol. 35, no. 33, pp. 23877-23891, 2023.

[28] O. S. Faragallah, H. M. El-Hoseny, and H. S. El-Sayed, "Efficient brain tumor segmentation using OTSU and K-means clustering in homomorphic transform," Biomedical Signal Processing and Control, vol. 84, p. 104712, 2023.

[29] S. R. Gunasekara, H. N. T. K. Kaldera, and M. B. Dissanayake, "A systematic approach for MRI brain tumor localization and segmentation using deep learning and active contouring," Journal of Healthcare Engineering, vol. 2021, 2021, doi: 10.1155/2021/6695108.

[30] A. Kumar, "Study and analysis of different segmentation methods for brain tumor MRI application," Multimedia Tools and Applications, vol. 82, no. 5, pp. 7117-7139, 2023, doi: 10.1007/s11042-022-13636-y.

APPENDIX

This appendix presents additional visual results of the brain tumor segmentation experiments described in the main text. Figures A1–A3 illustrate the top ten images segmented using the hybrid FCM-Otsu method, the FCM method, and the Otsu method, respectively, providing a visual comparison of the performance and effectiveness of each approach.

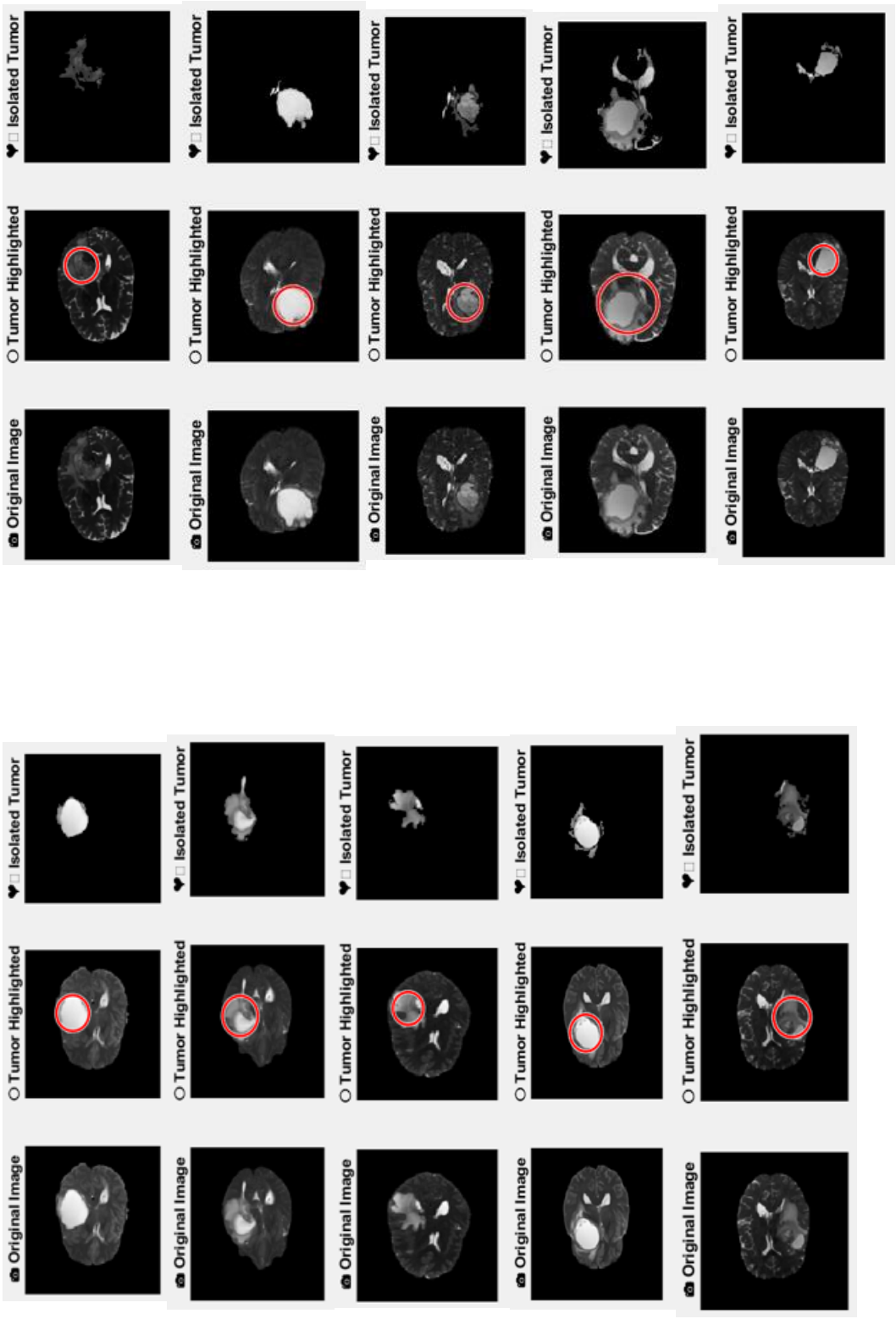

Figure A1: The segmentation image of the top ten images using the hybrid method.

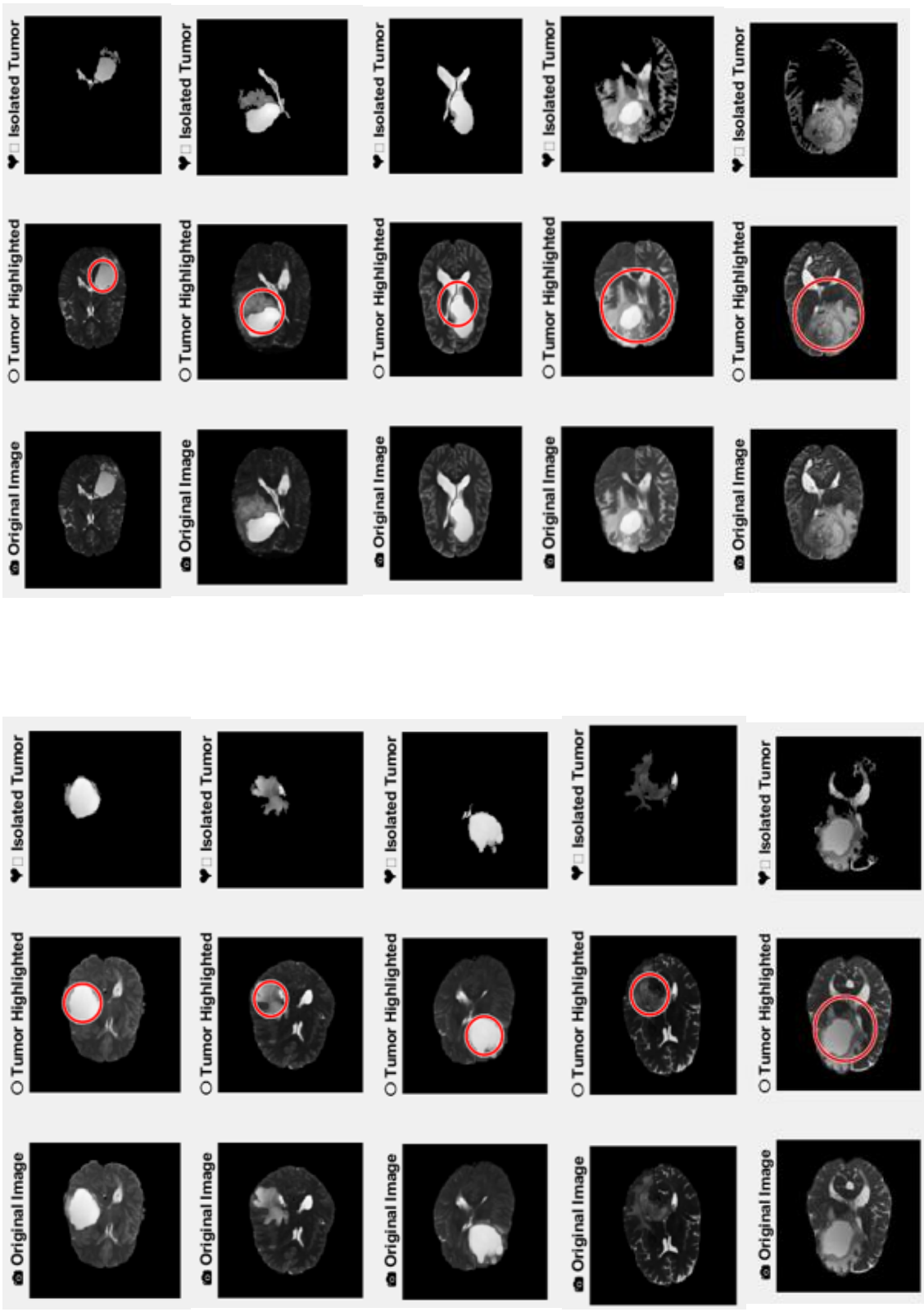

Figure A2: The segmented image of the top ten images using the Otsu method.

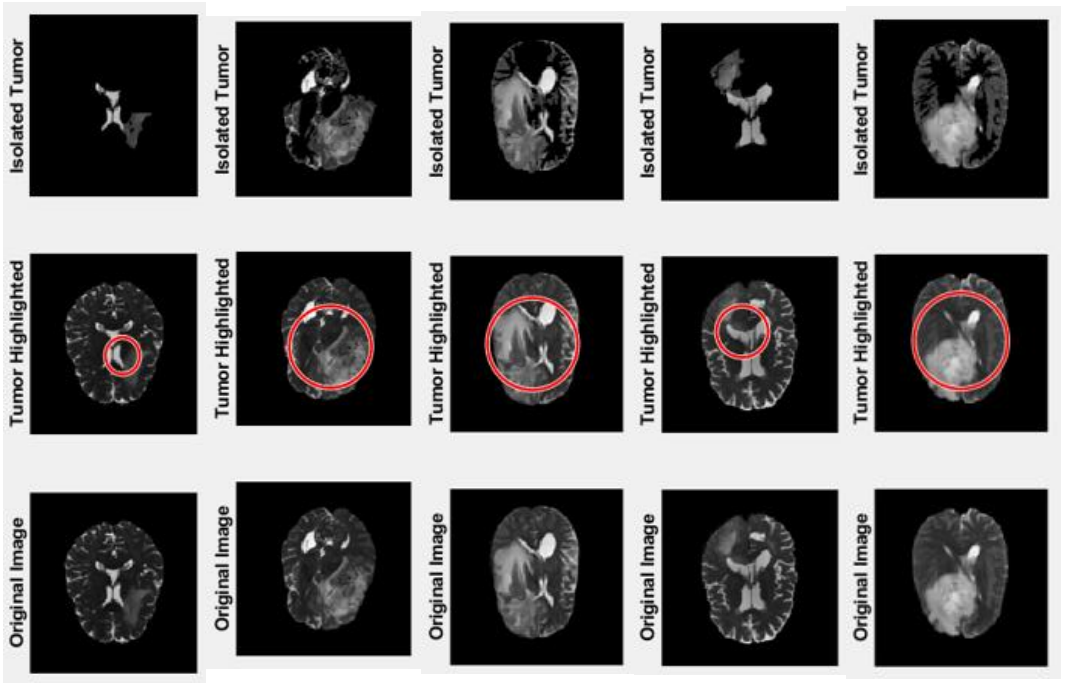

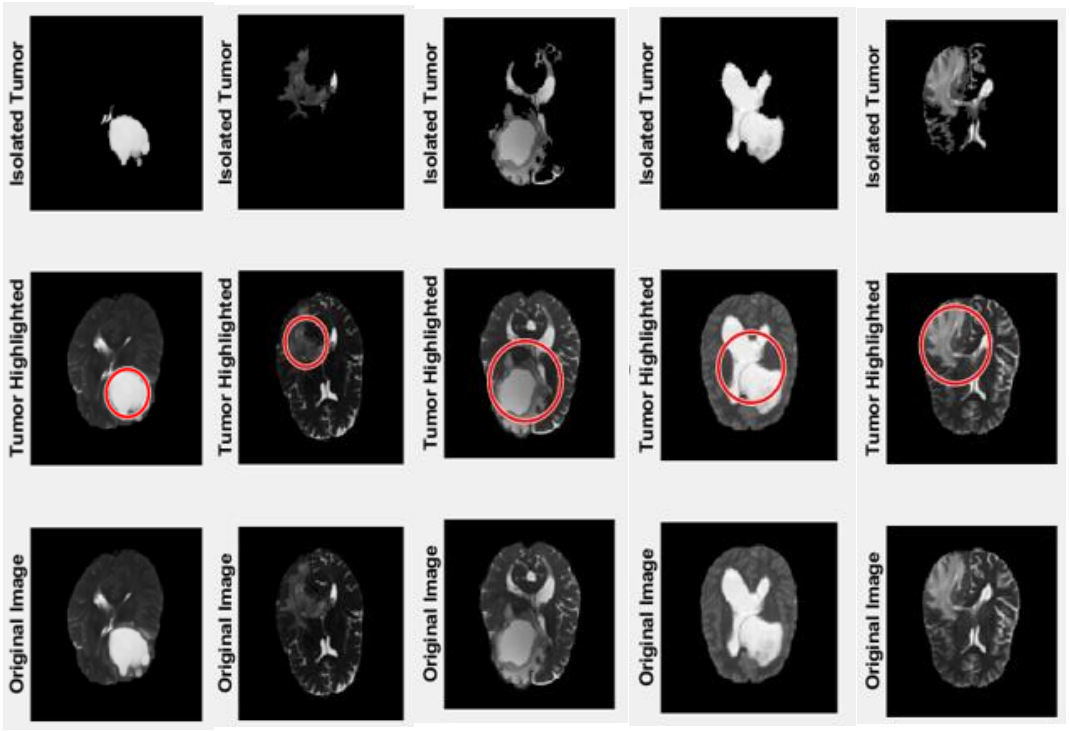

Figure A3: Segmentation image of the top ten images using the FCM method.